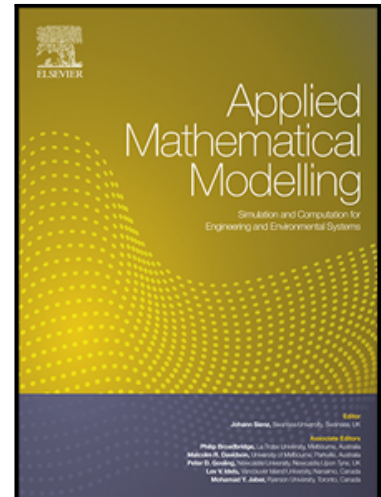


Journal Pre-proof

Model and performance analysis of non-uniform piezoelectric semiconductor nanofibers

Kai Fang , Peng Li , Nian Li , Dianzi Liu , Zhenghua Qian , Vladimir Kolesov , Iren Kuznetsova

PII: S0307-904X(21)00577-1
DOI: <https://doi.org/10.1016/j.apm.2021.12.009>
Reference: APM 14315



To appear in: *Applied Mathematical Modelling*

Received date: 10 August 2021
Revised date: 4 December 2021
Accepted date: 6 December 2021

Please cite this article as: Kai Fang , Peng Li , Nian Li , Dianzi Liu , Zhenghua Qian , Vladimir Kolesov , Iren Kuznetsova , Model and performance analysis of non-uniform piezoelectric semiconductor nanofibers, *Applied Mathematical Modelling* (2021), doi: <https://doi.org/10.1016/j.apm.2021.12.009>

This is a PDF file of an article that has undergone enhancements after acceptance, such as the addition of a cover page and metadata, and formatting for readability, but it is not yet the definitive version of record. This version will undergo additional copyediting, typesetting and review before it is published in its final form, but we are providing this version to give early visibility of the article. Please note that, during the production process, errors may be discovered which could affect the content, and all legal disclaimers that apply to the journal pertain.

© 2021 Published by Elsevier Inc.

Highlights

- The piezotronic fields in non-uniform piezo-semiconductive fibers are solved using a power series expansion method.
- The convergence and correctness of the method are proved.
- The antisymmetry of the electromechanical fields is broken due to the contoured profile.
- A necking heterogeneous piezoelectric semiconductor PN junction is more conveniently modulated.

Model and performance analysis of non-uniform piezoelectric semiconductor nanofibers

Kai Fang^{1,2}, Peng Li^{1,2}, Nian Li^{1,2}, Dianzi Liu³, Zhenghua Qian^{1,2,*}, Vladimir Kolesov⁴, Iren Kuznetsova⁴

¹ State Key Laboratory of Mechanics and Control of Mechanical Structures, College of Aerospace Engineering, Nanjing University of Aeronautics and Astronautics, Nanjing 210016, China

² Nanjing University of Aeronautics and Astronautics Shenzhen Research Institute, Shenzhen, 518057, China

³ School of Engineering, University of East Anglia, Norwich, UK

⁴ Kotel'nikov Institute of Radio Engineering and Electronics of RAS, Moscow 125009, Russia

*E-mail: qianzh@nuaa.edu.cn; zhenghua_qian@163.com

Tel.: +86-25-84895952, Fax: +86-25-84891422

Abstract: In order to evidently improve the working performance of piezotronic devices, non-uniform piezoelectric semiconductor fibers with contoured profiles are designed. However, apart from the finite element method, it's hard to achieve analytical descriptions of the electromechanical fields in these non-uniform piezoelectric semiconductor fibers because of the governing equations with variable coefficients. For solving this bottleneck and exploring improved performance and new phenomena caused by the non-uniform profile, a power series expansion method is proposed based on the framework of the one-dimensional linearized model and is further applied to analyze the piezotronic performances of n-type non-uniform piezoelectric semiconductor fibers and PN junctions. It is revealed via systematical numerical simulations that the antisymmetry of the electromechanical fields in piezoelectric semiconductor fibers is broken because of the contoured profile and the piezotronic coupling. Meanwhile, the barrier configuration in a non-uniform PN junction is sensitive to the variation of cross-sectional area. Furthermore, the current-voltage relation of a necking heterogeneous piezoelectric semiconductor PN junction can be manipulated more conveniently by external mechanical loadings, meaning that the sensitivity of the device is improved. Not limited by non-uniform piezoelectric semiconductor fibers with contoured profiles, this method exhibits broad applicability, which is still available for solving multiple-coupled properties of functional graded piezoelectric semiconductor media.

Keywords: contoured piezoelectric semiconductor, PN junction, power series expansion method, polarization, piezotronics.

1. Introduction

Recently, more and more piezoelectric semiconductive (PS) devices, such as nanogenerators [1, 2], piezotronic field-effect transistors [3, 4], piezotronic and chemical sensors [5-7], piezotronic logic nanodevices [8] and so forth, have been successfully developed and applied due to their unique coupling of piezoelectricity and semiconductor properties. Accompany with that, a new research area called piezotronics and piezophotonics has been formed. Different from the conventional semiconductors, the electric properties of PS devices can be tuned by applied mechanical loading, which is the main effect of piezotronic coupling [9-11].

When self-powered PS devices are applied as sensors, one of the most concerned issues is sensitivity. To improve their sensitivity to mechanical loading, materials with high piezoelectric constants and low dielectricity were developed since they are easier to produce higher piezoelectric fields [12, 13]. Another choice to obtain superior electric response is employing PS composite structures instead of single PS media [14, 15]. Recently, it has been revealed that non-uniform strain applied on the PS media can effectively improve the effective piezoelectric constant and then enhance the piezotronic performance [16], which brings new inspiration for the structural design of high sensitivity PS devices. As we all know, the simplest way to produce non-uniform strains in PS fibers is to employ a non-uniform shape with variable cross sections. Actually, a nanogenerator based on conical PS nanowires has been successfully fabricated, which can produce an output power that is strong enough to continuously drive a commercial liquid crystal [17]. Moreover, it was demonstrated via FEM analysis that tapered PS nanostructures can transduce tiny input mechanical forces into high piezo-potentials [18, 19]. Non-uniform PS structures show great potential in designing piezotronic devices with high sensitivity, hence

it is necessary to theoretically analyze their electromechanical properties, which is just the origin of this contribution.

The previous works about the non-uniform PS structures mentioned above are all based on conical fibers because it's easy for engineering implementation, as well as convenient for obtaining exact theoretical solutions. Actually, PS fibers with arbitrary contoured profiles are usually encountered during application. For example, unavoidable defects during mechanical processing or chemical and biological corrosion may lead to accidented surfaces. Sometimes, some particular variable profile patterns are designed with the aim of improving the sensitivity. Especially, with the development of modern micromachining, e.g., 3D printing technology, fabricating a non-uniform PS fiber at will is anticipated to achieve sooner and later. However, finding an theoretical solution beyond of FEM [20] to depict the electromechanical fields in a non-uniform PS fiber with random cross sections is still rare, which can't meet the design needs of engineers and scientists. In order to seek a general solution that is suitable for any non-uniform PS fibers with a random cross section, this paper presents a simple approach, i.e., the power series expansion method, to model and analyze the piezotronic performance of PS nanofibers, which is also the highlight of this contribution.

Firstly, the linearized one dimensional model for the non-uniform PS fibers is established in Section 2, which is based on the fully coupled theory of PS materials [21-26]. After that, a power series expansion method is proposed in Section 3 to solve the partial differential equation with variable coefficients that governs the carrier distributions in non-uniform PS fibers. In Section 4, the convergence of the power series expansion method is examined for three cases, one with a uniform n-type PS fiber and the other two with the cross-sectional area varying in linear and quadratic forms respectively. Then the influence of cross-sectional area variation on the electromechanical fields is investigated using fibers with linearly varying cross-sectional area as an example, and some novel phenomena induced are

revealed. Further, the power series expansion method is used to describe the piezotronic behavior of non-uniform PS PN junctions in Section 5. The improvement of sensitivity caused by junction necking is also investigated. Finally, the conclusions are summarized in Section 6.

2. One-dimensional Coupled Equations of a Contoured PS Fiber

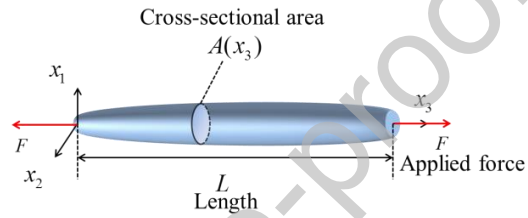


Fig. 1. Sketch of a non-uniform PS fiber with variable cross section.

In this paper, the usually used coupled-field theory consisting of the equations of linear piezoelectricity and charge conservation for electrons and holes is utilized to describe the electromechanical coupling properties of PS materials [27, 28], i.e.,

$$\begin{aligned}
 \sigma_{ij,j} &= \rho \frac{\partial^2 u_i}{\partial t^2}, \\
 D_{i,i} &= q(p - n + N_D^+ - N_A^-), \\
 J_{i,i}^p &= -q \frac{\partial p}{\partial t}, \\
 J_{i,i}^n &= q \frac{\partial n}{\partial t},
 \end{aligned} \tag{1}$$

where the Cartesian tensor notation has been used. σ_{ij} ($i, j = 1, 2, 3$), u_i and D_i are the stress tensor, mechanical displacement vector, and electric displacement vector, respectively. q represents the elementary charge, and ρ the mass density. p and n respectively stand for the concentrations of holes and electrons, with J_i^p and J_i^n being their individual current densities. Meanwhile, N_D^+ and N_A^- are the impurity concentration of donors and accepters. A comma followed by a suffix “,” and “,” respectively denote the derivative with respect to the coordinates x_i and x_j , and the repeated subscript indexes i and j represent the summation from 1 to 3. The partial derivative with respect to t represents the time derivative. Based on the assumption of zero net recombination rate, the constitutive relations can be expressed as

$$\begin{aligned}\sigma_{ij} &= c_{ijkl} S_{kl} - e_{kij} E_k, \\ D_i &= \varepsilon_{ij} E_j + e_{ijk} S_{jk}, \\ J_i^p &= qp\mu_{ij}^p E_j - qD_{ij}^p p_{,j}, \\ J_i^n &= qn\mu_{ij}^n E_j + qD_{ij}^n n_{,j}.\end{aligned}\tag{2}$$

Here c_{ijkl} , e_{kij} , ε_{ij} , μ_{ij}^p (μ_{ij}^n) and D_{ij}^p (D_{ij}^n) represent the elastic constants, piezoelectric constants, dielectric constants, carrier mobility, and carrier diffusion constants respectively. Meanwhile, the strain tensor S_{kl} and electric field vector E_j are controlled by the following strain-displacement relation and the electric field-potential relation

$$\begin{aligned}S_{ij} &= \frac{1}{2}(u_{i,j} + u_{j,i}), \\ E_i &= -\varphi_{,i}.\end{aligned}\tag{3}$$

The electron and hole concentrations can be written as:

$$\begin{aligned}p &= p_0 + \Delta p, \quad n = n_0 + \Delta n, \\ p_0 &= N_A^-, \quad n_0 = N_D^+, \end{aligned}\tag{4}$$

where Δn and Δp are perturbations of the carrier concentrations, and n_0 and p_0 denote the initial carrier concentrations in the reference state before stress applied. Considering the case of uniform doping with small Δp and Δn , the first n and p in Eq. (2) can be written as n_0 and p_0 . Then the nonlinear terms of n and p in the last two equations of (2) are linearized such that n_j and p_j are linear correlations to E_j . Some expressions in Eqs. (1) and (2) become:

$$\begin{aligned} D_{i,i} &= q(\Delta p - \Delta n), \\ q \frac{\partial}{\partial t} (\Delta p) &= -J_{i,i}^p, \\ q \frac{\partial}{\partial t} (\Delta n) &= J_{i,i}^n. \end{aligned} \quad (5)$$

$$\begin{aligned} J_i^p &= qp_0 \mu_{ij}^p E_j - qD_{ij}^p (\Delta p)_{,j}, \\ J_i^n &= qn_0 \mu_{ij}^n E_j + qD_{ij}^n (\Delta n)_{,j}. \end{aligned} \quad (6)$$

Consider the extensional deformation of a non-uniform PS fiber with variable circular cross section shown in Fig. 1, the fiber length is L and the x_3 coordinate locates along the central line with its origin at the left end surface. The variable cross-sectional area is represented by a random function $A(x_3)$ and a pair of extensional forces F are applied at the two ends. For the equilibrium and the steady states considered, the governing equations become [20]:

$$\begin{aligned} (A\sigma_{33})_{,3} &= [A(\bar{c}_{33}u_{,3,3} + \bar{e}_{33}\varphi_{,3})]_{,3} = 0, \\ (AD_3)_{,3} &= [A(\bar{e}_{33}u_{,3,3} - \bar{\epsilon}_{33}\varphi_{,3})]_{,3} = -qA(\Delta n - \Delta p), \\ (AJ_3^n)_{,3} &= [A(-qn_0\mu_{33}^n\varphi_{,3} + qD_{33}^n\Delta n_{,3})]_{,3} = 0, \\ (AJ_3^p)_{,3} &= [A(-qp_0\mu_{33}^p\varphi_{,3} - qD_{33}^p\Delta p_{,3})]_{,3} = 0. \end{aligned} \quad (7)$$

Here \bar{c}_{33} , \bar{e}_{33} and $\bar{\epsilon}_{33}$ are the effective one-dimensional elastic, piezoelectric, and dielectric constants introduced by the one-dimensional stress relaxation condition [29], i.e.,

$$\begin{aligned}
 \bar{c}_{33} &= 1/s_{33}^E, \\
 \bar{e}_{33} &= d_{33}/s_{33}^E, \\
 \bar{\epsilon}_{33} &= \epsilon_{33}^T - d_{33}^2/s_{33}^E.
 \end{aligned} \tag{8}$$

The isolated boundary condition at two ends $x_3 = L$ and $x_3 = 0$ require $J_3^n = J_3^p = 0$ in Eq. (7), thus:

$$\begin{aligned}
 \Delta n_{,3} &= n_0 \frac{\mu_{33}^n}{D_{33}^n} \varphi_{,3}, \\
 \Delta p_{,3} &= -p_0 \frac{\mu_{33}^p}{D_{33}^p} \varphi_{,3}.
 \end{aligned} \tag{9}$$

Subtracting these two equations from each other, we have:

$$(\Delta n - \Delta p)_{,3} = \left(n_0 \frac{\mu_{33}^n}{D_{33}^n} + p_0 \frac{\mu_{33}^p}{D_{33}^p} \right) \varphi_{,3}. \tag{10}$$

It should be stressed that the carried mobility μ_{33}^n (μ_{33}^p) and the carrier diffusion constants D_{33}^n (D_{33}^p) in Eq. (10) satisfy the Einstein relation, i.e.,

$$\frac{\mu_{33}^n}{D_{33}^n} = \frac{\mu_{33}^p}{D_{33}^p} = \frac{q}{k_B T}, \tag{11}$$

with the Boltzmann constant k_B and the absolute temperature T . We note from the first equation in Eq. (7) that the axial force $A\sigma_{33}$ is a constant. Therefore, the mechanical boundary conditions at $x_3 = L$ and $x_3 = 0$ require $A\sigma_{33} = F$, and then we can obtain

$$u_{3,3} = \frac{F}{\bar{c}_{33}A} - \frac{\bar{e}_{33}}{\bar{c}_{33}} \varphi_{,3} = \frac{F}{\bar{c}_{33}A} - \frac{\bar{e}_{33}}{\bar{c}_{33}} \frac{1}{n_0 \frac{\mu_{33}^n}{D_{33}^n} + p_0 \frac{\mu_{33}^p}{D_{33}^p}} (\Delta n - \Delta p)_{,3}. \tag{12}$$

Substituting Eqs. (10) and (12) into the second equation of Eq. (7), we get a differential equation with variable coefficients:

$$A(\Delta n - \Delta p)_{,33} + A_{,3}(\Delta n - \Delta p)_{,3} - \kappa^2 A(\Delta n - \Delta p) = 0 \quad (13)$$

with

$$\kappa^2 = \frac{q(n_0 \frac{\mu_{33}^n}{D_{33}^n} + p_0 \frac{\mu_{33}^p}{D_{33}^p})}{\bar{\epsilon}_{33} (\frac{\bar{e}_{33}^2}{c_{33} \bar{\epsilon}_{33}} + 1)}, \quad (14)$$

which controls the electrical performance of a contoured PS fiber under extension.

3. Power Series Expansion for the Partial Differential Equation with Variable Coefficients

Eq. (13) is a partial differential equation with variable coefficients, for which exact analytical solution is available only for some specific forms of cross-sectional area variation function $A(x_3)$. The aim of this paper is to seek a general theoretical solution applicable to an arbitrary contour shape. Motivated by Taylor series, a known one-dimensional function can be written into a power series. Despite of unknown $\Delta n - \Delta p$ and random $A(x_3)$, they still can be expressed as

$$A = [A_0 + A_1 (\frac{x_3}{L}) + A_2 (\frac{x_3}{L})^2 + \dots] = \sum_{s=0}^{M_s} A_s (\frac{x_3}{L})^s, \quad (15)$$

$$\Delta n - \Delta p = [N_0 + N_1 (\frac{x_3}{L}) + N_2 (\frac{x_3}{L})^2 + \dots] = \sum_{z=0}^{M_z} N_z (\frac{x_3}{L})^z,$$

where M_s and M_z are the series truncation parameters. A_s is determined by the cross-sectional area variation function and N_z will be determined afterwards. Substitute Eqs. (15) into Eq. (13) yields:

$$\sum_{s=0}^{M_s} A_s (\frac{x_3}{L})^s \sum_{z=2}^{M_z} \frac{1}{L^2} z(z-1) N_z (\frac{x_3}{L})^{z-2} + \frac{1}{L^2} \sum_{s=1}^{M_s} s A_s (\frac{x_3}{L})^{s-1} \sum_{z=1}^{M_z} z N_z (\frac{x_3}{L})^{z-1} - \kappa^2 \sum_{s=0}^{M_s} A_s (\frac{x_3}{L})^s \sum_{z=0}^{M_z} N_z (\frac{x_3}{L})^z = 0. \quad (16)$$

Eq. (16) should be valid for arbitrary x_3 , which requires that the coefficients of $(x_3/L)^2$ must be zero. This leads to:

$$\sum_{s=0}^z \frac{1}{L^2} A_s (z-s+2)(z-s+1) N_{z-s+2} + \sum_{s=0}^z \frac{1}{L^2} (s+1) A_{s+1} (z-s+1) N_{z-s+1} - \kappa^2 \sum_{s=0}^z A_s N_{z-s} = 0. \quad (17)$$

Then, the recursive linear equation for N_z can be expressed as:

$$N_{z+2} = \frac{\kappa^2 \sum_{s=0}^z A_s N_{z-s} - \sum_{s=0}^z \frac{1}{L^2} (s+1) A_{s+1} (z-s+1) N_{z-s+1} - \sum_{s=0}^{z-1} \frac{1}{L^2} A_{s+1} (z-s+1)(z-s) N_{z-s+1}}{\frac{1}{L^2} A_0 (z+2)(z+1)}. \quad (18)$$

From Eq. (18), we note that there are totally two undetermined coefficients, i.e., N_0 and N_1 . Other coefficients N_z for $z > 1$ can be calculated using Eq. (18). In addition, we get from Eq. (18) that:

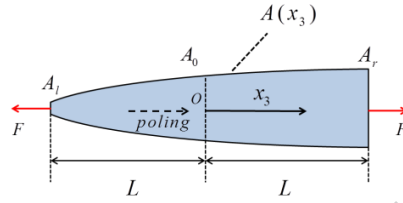
$$\lim_{z \rightarrow \infty} \left| \frac{N_{z+2}}{N_{z+1}} \right| = \lim_{z \rightarrow \infty} \left| \frac{(z+1)A_1}{(z+2)A_0} \right| = \left| \frac{A_1}{A_0} \right|. \quad (19)$$

Therefore, the power series solution is convergent as long as $|A_1| < |A_0|$ is ensured beforehand. Until now, we've obtained the semi-analytical solution to the partial differential equation (13), which will be used to describe the electromechanical fields in PS media.

4. Piezotronic Behaviors of Non-uniform N-type PS Fibers

In order to illustrate the generality and applicability of the power series expansion method deduced above, Eq. (15) is adopted to solve the electromechanical fields in the non-uniform n-type ZnO fiber shown in Fig. 2, in which the origin of the x_3 coordinate locates at the middle of the fiber. The material

constants of ZnO are listed in Table 1. Besides, the parameters used in this section to calculate the electromechanical fields of the n-type PS fibers are shown in Table 2 unless otherwise stated.



(b)

Fig. 2. N-type PS fiber with variable cross sections

Table 1

Material constants of ZnO [30].

Notation	Description	Value
s_{33}^E	Elastic compliance constant	$6.94 \times 10^{-12} \text{ m}^2/\text{N}$
d_{33}	Piezoelectric constant	$11.67 \times 10^{-12} \text{ C/N}$
ϵ_{33}^T	Dielectric constant	$1.12 \times 10^{-10} \text{ F/m}$
q	Elementary charge	$1.60218 \times 10^{-19} \text{ C}$
$k_B T/q$	Thermal voltage at 300 K	0.0259 V

Table 2

Parameter settings for the n-type fibers in Section 4.

Notation	Description	Value
----------	-------------	-------

L	Length of the the left and right halves	1 μm
A_r	Area of the right end surface	$2.598 \times 10^{-14} \text{ m}^2$
A_l	Area of the left end surface	Varies with function $A(x_3)$
F	Applied end force	2 nN
n_0	Initial electron concentration	$n_0 = 10^{21} /\text{m}^3$ [30]

4.1 Degenerated equations for non-uniform n-type PS fibers

For n-type PS materials, hole concentrations are neglected, i.e., the Δp and p_0 terms in Sections 2 and 3 vanish. Then, Eq. (13) becomes

$$A\Delta n_{,33} + A_{,3}\Delta n_{,3} - \kappa^2 A\Delta n = 0, \quad (20)$$

and the perturbation of the carrier concentration Δn reduces as

$$\Delta n = [N_0 + N_1\left(\frac{x_3}{L}\right) + N_2\left(\frac{x_3}{L}\right)^2 + \dots] = \sum_{z=0}^{M_z} N_z \left(\frac{x_3}{L}\right)^z. \quad (21)$$

For the isolated n-type PS fiber in Fig. 2, two boundary conditions are enough to determine the unknown coefficients N_0 and N_1 in Eq. (21), and the electrical open-circuit boundaries at $x_3 = \pm L$ are considered, i.e.

$$D_3(L) = \frac{F\bar{e}_{33}}{A\bar{c}_{33}} - \left(\frac{\bar{e}_{33}\bar{e}_{33}}{\bar{c}_{33}} + \bar{\varepsilon}_{33}\right) \frac{1}{n_0 \frac{\mu_{33}^n}{D_{33}^n}} \sum_{z=1}^{M_z} \frac{1}{L} z N_z = 0, \quad (22)$$

$$D_3(-L) = \frac{F\bar{e}_{33}}{A\bar{c}_{33}} - \left(\frac{\bar{e}_{33}\bar{e}_{33}}{\bar{c}_{33}} + \bar{\varepsilon}_{33}\right) \frac{1}{n_0 \frac{\mu_{33}^n}{D_{33}^n}} \sum_{z=1}^{M_z} \frac{1}{L} z N_z (-1)^{z-1} = 0.$$

With the aid of Eqs. (9), (12) and (21), the electric field distribution E_3 and the strain distribution S_{33} can be calculated. However, with the known E_3 , a potential reference point is needed to uniquely determine the potential distribution φ . In some relevant literatures [31, 32], this potential reference point can be chosen anywhere in the fiber because it does not influence the carrier distributions physically. In present paper, we are particularly interested in the potential distribution, so the state before stress applied is chosen as the reference state. Hence, the relation between the potential and carrier concentration can be expressed as [33]:

$$n = n_0 \exp\left(\frac{q\varphi}{k_B T}\right), \quad (23)$$

which can be used to quantitatively calculate the potential distribution φ .

4.2 Convergence of the power series expansion method

The convergence of the method should be examined first to ensure computational accuracy. Table 3 displays the values of coefficient N_1 for some selected truncation parameters M_z for three different types of profile pattern, i.e., a uniform form with $A(x_3) = A_0$, a linear form with $A(x_3) = A_0(1 + \alpha_1 x_3/L)$, and a quadratic form with $A(x_3) = A_0(1 + \alpha_2 x_3/L)^2$. In simulations, the area ratio of the left end surface to the right end surface A_l/A_r is set to 0.4. It shows that the series produce stable results with about 30 series terms kept. In this paper, 50 terms in the series are adopted to obtain adequate accuracy in the following simulations.

Table 3

Coefficient N_1 for different truncations M_z .

$A(x_3) = A_0$		$A(x_3) = A_0(1+\alpha_1x_3/L)$		$A(x_3) = A_0(1+\alpha_2x_3/L)^2$	
M_z	$N_1 (\times 10^{18})$	M_z	$N_1 (\times 10^{17})$	M_z	$N_1 (\times 10^{17})$
20	3.70845	20	3.75782	20	3.84100
22	3.70798	22	3.75729	22	3.84030
24	3.70793	24	3.75722	24	3.84021
26	3.70792	26	3.75721	26	3.84020
28	3.70792	28	3.75721	28	3.84020
30	3.70792	30	3.75721	30	3.84020

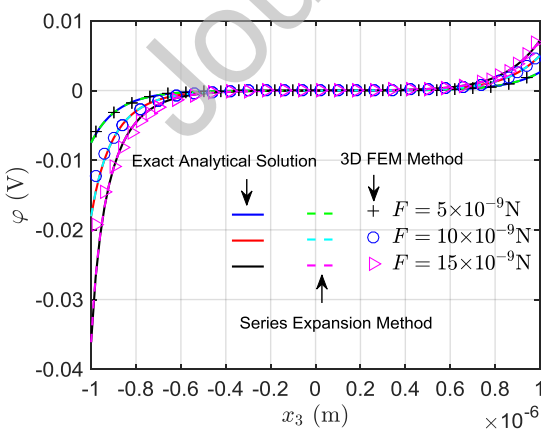
4.3 Numerical validation of the power series expansion method for non-uniform n-type fibers

Before analyzing the piezotronic performance of the non-uniform PS fiber, it is crucial and necessary to verify the power series expansion method and the linearized non-uniform model. It is found that for a special profile function $A(x_3) = A_0(1+\alpha_2x_3/L)^2$, it's easy to obtain an exact analytical solution of Eq. (20) without using the power series expansion method (details are shown in Appendix A). In addition, both the exact analytical solution and the power series expansion method we used are based on the 1D linearized equations, whose precision for describing an actual 3D PS fiber needs to be clarified. Therefore, Fig. 3(a) gives the electric potential φ distribution respectively from the exact analytical solution, the power series expansion method and the nonlinear 3D FEM simulation (details in Appendix B) for some selected applied forces when $A_l/A_r = 0.4$. The results from the exact analytical solution and the power series expansion method agree excellently well with each other, proving the

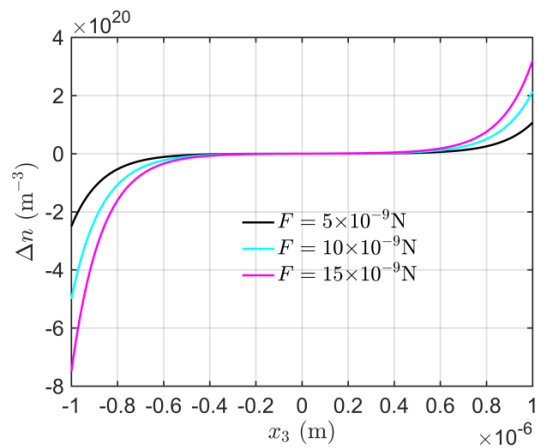
correctness of the theoretical method. However, when F is relatively large, the potential at the left end (smaller tip) calculated by 3D FEM software deviates from those obtained by the other two analytical methods, which is mainly caused by the following two reasons:

(1) The linearized model we used gives accurate results only when the carrier concentration perturbation Δn is relatively small (compared with the initial carrier concentration n_0). When $F = 15$ nN, Δn at the left end reaches up to $8 \times 10^{20} \text{ m}^{-3}$ (shown in Fig. 3(b)), which is about 0.8 times of the initial carrier concentration. The linearized model is acceptable when $|\Delta n| < 0.5n_0$. Therefore, the discrepancy between the present results and those of FEM occurs near the ends when $F = 15$ nN.

(2) The cross section of a 3D PS fiber is a 2D circular plane, in which the electric potential distribution is non-uniform, as shown in Fig. A1 in Appendix B. This actual inhomogeneous distribution is induced by two transverse strains in x_1 - x_2 plane via Poisson's effect. However, this phenomenon has been ignored in the linearized one-dimensional model with only the axial strain S_{33} considered, which inevitably leads to some deviations of the results. Nevertheless, when F is relatively small, these tiny deviations are negligible, meaning that the power series expansion method adopted here is accurate enough to conduct the following analysis.



(a)



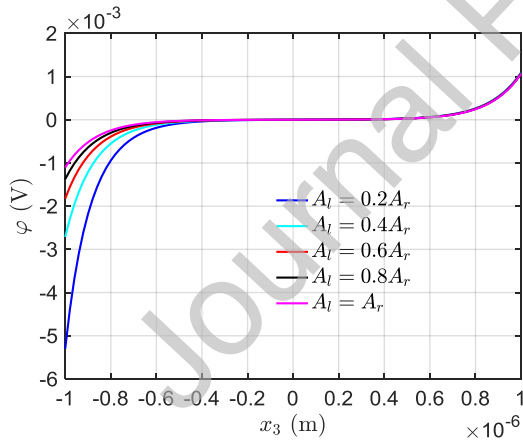
(b)

Fig. 3. (a) The distribution of electric potential φ calculated by different methods; (b) The corresponding carrier concentration variation Δn .

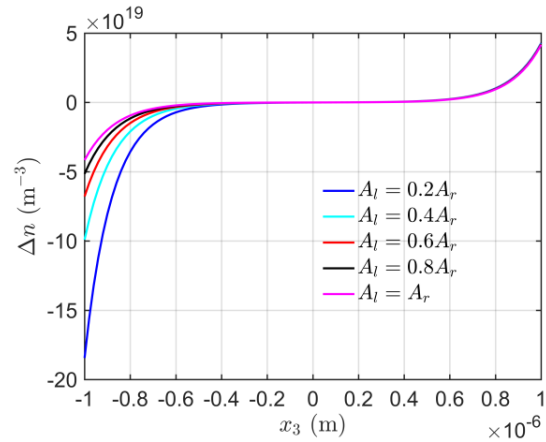
4.4 Influence of the cross-sectional area variation of non-uniform n-type fibers

Next, we will choose a linear cross-sectional area variation $A(x_3) = A_0(1 + \alpha_1 x_3/L)$ as an example to explore some interesting piezotronic performances of the n-type non-uniform PS fiber. Figs. 4(a) and 4(b) show the distributions of electric potential φ and the carrier concentration variation Δn along the x_3 axis for different values of area ratio A_l/A_r , in which $A_l = A_r$ corresponds to uniform fibers while $A_l \neq A_r$ stands for non-uniform fibers with variable cross sections. As expected, after applying the axial force F , electrons are driven to one end of the fiber, and the piezo-potential is partially screened by free carriers, resulting in mainly flat middle parts of the potential curves. This phenomenon exists in both uniform and non-uniform fibers and presents the typical piezotronic coupling, i.e., the mechanically induced redistribution of mobile charges. However, new performance, the antisymmetry destruction, appears only in non-uniform fibers. In (a) and (b), we see that the distributions of φ and Δn are antisymmetric about $x_3 = 0$ for a uniform fiber ($A_l = A_r$). Generally, as the applied force F increases, this antisymmetry will be gradually broken [33]. However for non-uniform PS fibers ($A_l \neq A_r$), this antisymmetry can be broken even under a much smaller applied force F , and it depends on the area ratio A_l/A_r . For example, for a smaller A_l/A_r (a thinner left tip) in (a) and (b), the piezo-potential and carrier concentration at the left end vary more rapidly and dramatically than those at the right end. Even when the piezo-potential near the thinner end increases 5 times as the surface area decreases, the potential and carrier concentration variation near the thicker end hardly change. A detailed explanation of this phenomenon will be given in the next paragraph. (c) and (d) show the distributions of strain S_{33} and polarization P . It

can be seen that a substantially larger strain is always produced at the narrow tip (the left tip when $A_l < A_r$), and thus gives a larger polarization in this zone via piezoelectric effect. In addition, the electric distribution φ for different values of initial carrier concentration n_0 when $A_l = 0.2A_r$ is plotted in Fig. 4(e). With the decrease of n_0 , electric potential φ near the two ends increases, and the antisymmetry broken becomes more severe. This is because there are not enough free carriers to screen the piezo-potential when n_0 is small. As n_0 is down to 10^{18} m^{-3} , the non-uniform PS fiber performs like a dielectric without free carriers. Therefore, we can deem 10^{18} m^{-3} as a criterion of n_0 , beyond which the semiconductive property should be taken into account. Fig. 4(f) shows the potential difference $\Delta\varphi$ between the two ends of the fiber for both compressive and tensile stresses. It can be found that the potential-force relation is non-antisymmetric and nonlinear, which is quite different from that of an insulating piezoelectric fiber (strictly antisymmetric and linear) and mainly owes to both the geometry and the piezotronic coupling.



(a)



(b)

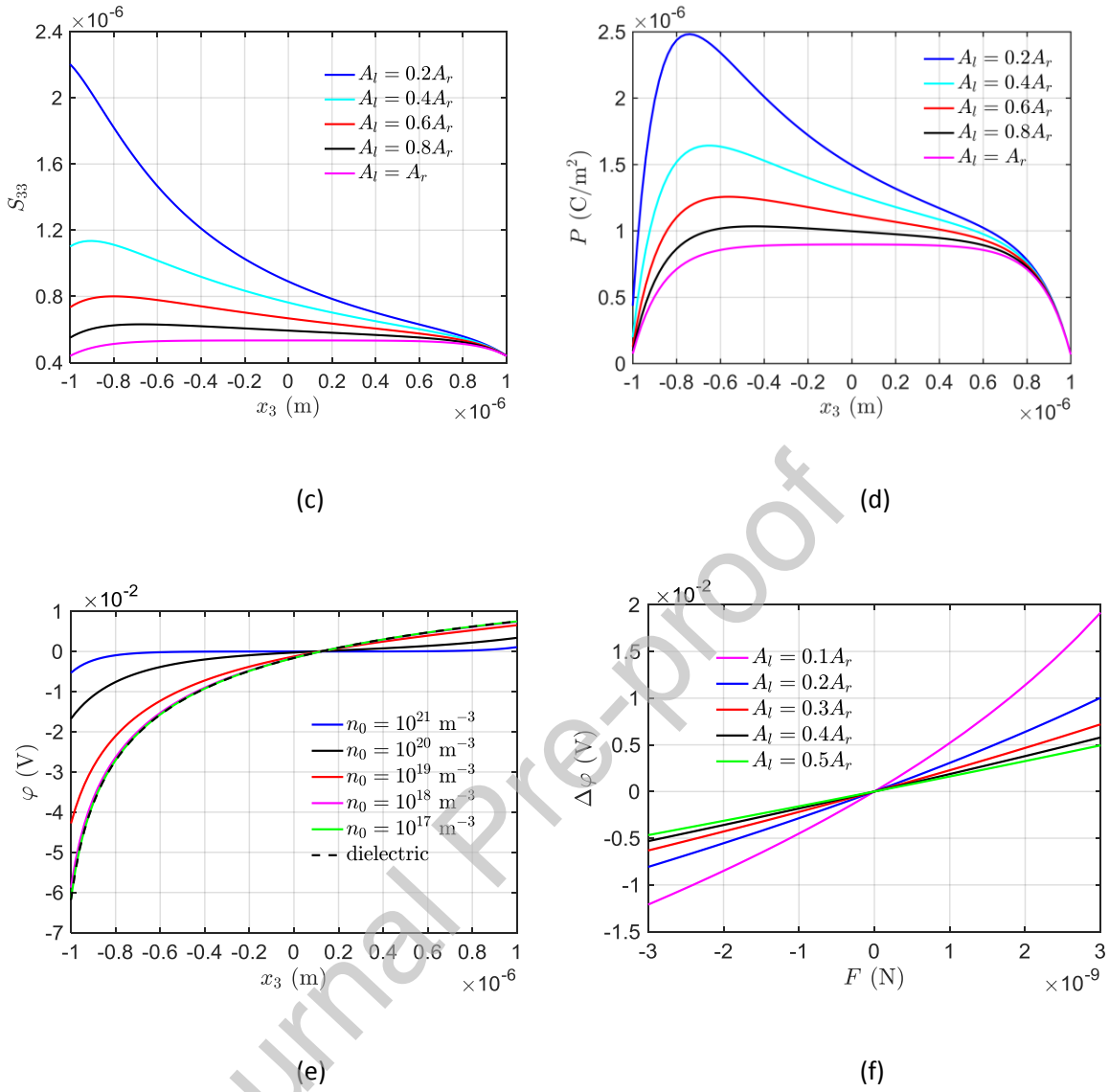


Fig. 4 (a) Electric potential φ , (b) carrier concentration variation Δn , (c) axial strain S_{33} and (d) polarization P along the axis for different values of area ratio A_l / A_r , $F=2$ nN. (e) Electric potential φ along the axis when initial carrier concentration n_0 varies. (f) Potential difference $\Delta\varphi$ between the two ends $x_3 = \pm L$ versus applied force F .

It is known that polarization charges appear at the polarization discontinuities. Therefore, there exist surface polarization charges with a density $\rho_s = \mathbf{P} \cdot \mathbf{n}$ [34] per unit area at both end surfaces of the fiber. Then the total surface charge Q_s can be calculated by $\rho_s \cdot A$. To clearly reveal the reason for the antisymmetry broken of the electromechanical fields in non-uniform PS fibers, we list the values of ρ_s and Q_s for different values of A_l / A_r in Table 4. It can be seen that positive charges appear on the right end surface while negative charges on the left. Since electrons in n-type fibers are negatively charged, they will be driven away from the negative polarization charges on the left surface and attracted to the positive charges on the right by electrostatic forces, which is consistent with the Δn distribution in Fig. 4(b). At the left end, both the absolute values of ρ_s and Q_s increase as the surface area shrinks. By contrast, they vary quite slightly at the right end. This is because the deformation of the thinner left end is much larger than the thicker right end when subjected to an axial loading, and thus producing a larger polarization there via piezoelectric effect. Accordingly, more free electrons are redistributed near the left end compared to the right, and further causes a more dramatic variation of the electromechanical fields there. This unique antisymmetry broken is useful for designing piezotronic devices with high on-off ratios.

Table 4

Surface charge density ρ_s and surface charge Q_s on the left and right end surfaces.

A_l / A_r	$\rho_s(-L) (\times 10^{-7} \text{ C/m}^2)$	$\rho_s(L) (\times 10^{-8} \text{ C/m}^2)$	$Q_s(-L) (\times 10^{-21} \text{ C})$	$Q_s(L) (\times 10^{-21} \text{ C})$
1	-0.7410	6.8185	-1.9252	1.7715
0.8	-0.9360	6.8167	-1.9454	1.7710
0.6	-1.2698	6.8148	-1.9793	1.7705
0.4	-1.9708	6.8129	-2.0480	1.7700

0.2	-4.3542	6.8109	-2.2624	1.7695
-----	---------	--------	---------	--------

5. Piezotronic Behaviors of Non-uniform PS PN Junctions

To further demonstrate the versatility of the power series expansion method and exploring new physical phenomena caused by PS fiber's contoured profile, the piezotronic behaviors of non-uniform PS PN junctions are analyzed here. Consider two kinds of non-uniform ZnO PS PN junctions shown in Fig. 5, the top one is a homogeneous junction with a uniform c -axis throughout the fiber, while the bottom one is a heterogeneous junction with opposite c -axes in the two halves. The parameters used for the PN junctions in this section are listed in Table 5, where the superscripts ' l ' and ' r ' respectively denote the quantities in the left and the right regions of the junction, i.e., $x_3 < 0$ and $x_3 \geq 0$.

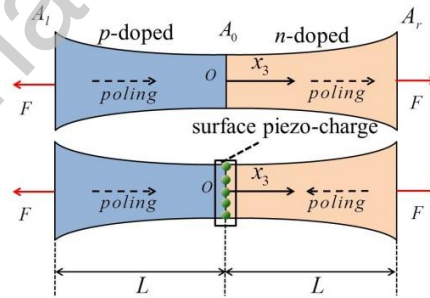


Fig. 5. Non-uniform homogeneous and heterogeneous PS PN junctions

Table 5

Parameter settings for the PN junctions in Section 5

Notation	Description	Value
L	Length of the the left and right halves	2 μm
A_r	Area of the right end surface	$2.598 \times 10^{-14} \text{ m}^2$
A_l	Area of the left end surface	$2.598 \times 10^{-14} \text{ m}^2$
A_0	Cross-sectional area at the origin	Varies with function $A(x_3)$
F	Applied end force	7 nN
n_0^r	Initial electron concentration of the n -doped zone	$10^{21} / \text{m}^3$ [35]
p_0^l	Initial hole concentration of the p -doped zone	$10^{21} / \text{m}^3$ [35]
n_0^l	Initial electron concentration of the p -doped zone	$7 \times 10^{20} / \text{m}^3$ [35]
p_0^r	Initial hole concentration of the n -doped zone	$7 \times 10^{20} / \text{m}^3$ [35]

5.1 Equations for non-uniform PS PN junctions

In PN junctions, holes (electrons) are driven from the p-zone (n-zone) to the n-zone (p-zone), forming a space charge region near the interface between them. Because of this, the electromechanical fields in PN junctions are more complex than those in pure n-type or p-type fibers. Taking the region $x_3 \geq 0$ (denoted by superscripts 'r') for instance, Eq. (10) gives

$$\varphi = \frac{1}{\left(n_0^r \frac{\mu_{33}^{nr}}{D_{33}^{nr}} + p_0^r \frac{\mu_{33}^{pr}}{D_{33}^{pr}}\right)} (\Delta n - \Delta p) + C_1, \quad (24)$$

with an undetermined constant C_1 . Using the power series expressed in Eq. (15), Eq. (24) becomes

$$\varphi = \frac{1}{\left(n_0^r \frac{\mu_{33}^{nr}}{D_{33}^{nr}} + p_0^r \frac{\mu_{33}^{pr}}{D_{33}^{pr}}\right)} \sum_{z=0}^{M_z} N_z^r \left(\frac{x_3}{L}\right)^z + C_1. \quad (25)$$

Combining Eq. (25) with the first equation in (9), we have:

$$\begin{aligned} \Delta n &= n_0^r \frac{\mu_{33}^{nr}}{D_{33}^{nr}} \frac{1}{\left(n_0^r \frac{\mu_{33}^{nr}}{D_{33}^{nr}} + p_0^r \frac{\mu_{33}^{pr}}{D_{33}^{pr}}\right)} \sum_{z=0}^{M_z} N_z^r \left(\frac{x_3}{L}\right)^z + n_0^r \frac{\mu_{33}^{nr}}{D_{33}^{nr}} C_1 + C_2, \\ \Delta p &= \left(n_0^r \frac{\mu_{33}^{nr}}{D_{33}^{nr}} \frac{1}{\left(n_0^r \frac{\mu_{33}^{nr}}{D_{33}^{nr}} + p_0^r \frac{\mu_{33}^{pr}}{D_{33}^{pr}}\right)} - 1\right) \sum_{z=0}^{M_z} N_z^r \left(\frac{x_3}{L}\right)^z + n_0^r \frac{\mu_{33}^{nr}}{D_{33}^{nr}} C_1 + C_2, \end{aligned} \quad (26)$$

in which C_2 is the undetermined constant. Similarly, general solutions for $x_3 \leq 0$ can also be derived with two another undetermined constants C_3 and C_4 . Until now, eight unknown constants $N_0^r, N_1^r, N_0^l, N_1^l, C_1, C_2, C_3$ and C_4 exist, which will be determined through the following boundary conditions:

$$\begin{aligned} D_3(L) &= 0, \quad D_3(-L) = 0, \quad D_3(0^+) = D_3(0^-), \\ \varphi(0^+) &= \varphi(0^-) = 0, \quad n(0^-) = n(0^+), \quad p(0^-) = p(0^+). \end{aligned} \quad (27)$$

In addition, Δp and Δn must satisfy the global charge neutrality conditions [11, 36], i.e.,

$$\int_{-L}^L A \Delta n dx = 0, \quad \int_{-L}^L A \Delta p dx = 0. \quad (28)$$

Only one of Eq. (28) is independent. So far, we have eight boundary conditions, enough to determine all the unknown constants in Eqs. (24), (25), and (26). After that, the electromechanical fields in PS/PN junctions can be obtained.

5.2 Numerical validation of the power series expansion method for PS/PN junctions

We note that a homogeneous PN junction will degenerate into the n-type fiber studied in Section 4 if the doping profile is chosen to be $n'_0 = n'_r = 10^{21} \text{ m}^{-3}$ and $p'_0 = p'_r = 0$. Based on this fact, the numerical example in Section 4.4 will be calculated again using the equations in Section 5.1, and then their results will be compared with each other to validate the power series expansion method for PN junctions deduced here. The comparison of the electric potential φ for some selected profiles is shown in Fig. 6. The curves agree very well with each other, indicating that the power series expansion method here is still valid for the multi-coupled analysis for PS PN junctions.

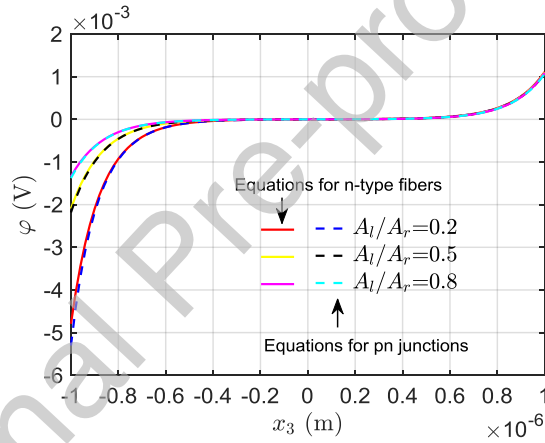


Fig. 6. A comparison of the electric potential φ calculated using the equations for n-type fibers with that using the equations for PN junctions.

5.3 Influence of the cross-sectional area variation of non-uniform PS PN junctions

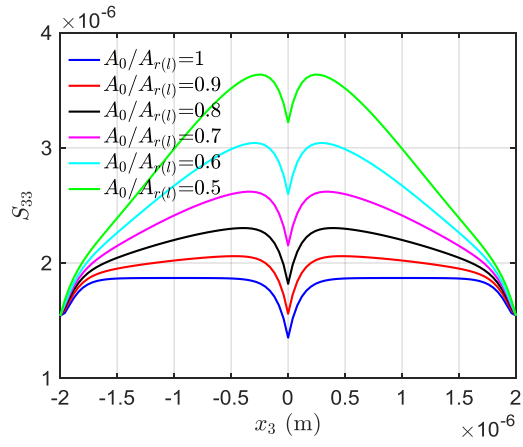
In this subsection, the cross-sectional area variation function $A(x) = A_0 + A_0 \alpha (x_3/L)^2$ is chosen as an example to study the influence of profile on the piezotronic behavior of non-uniform PS PN junctions.

The profile has been shown in Fig. 5, which is symmetric about $x_3 = 0$, so in following analysis the surface areas of the two ends A_l and A_r are kept constant as $2.598 \times 10^{-14} \text{ m}^2$, while the interface area A_0 is variable.

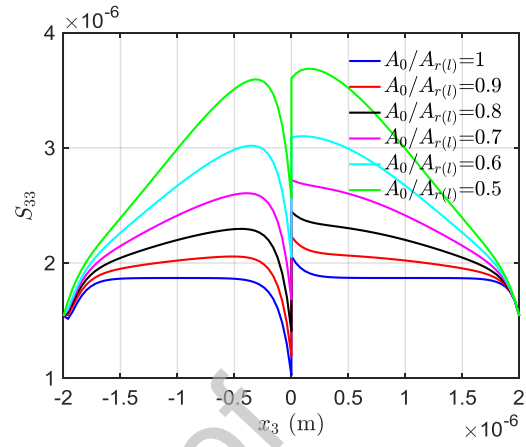
Firstly, the distribution of axial strain S_{33} in homogeneous and heterogeneous junctions are examined in Figs. 7(a) and 7(b), respectively. As expected, subject to a pair of constant applied forces, a smaller $A_0/A_{r(l)}$ (a narrower fiber) corresponds to a larger strain and the largest strain always locates at the thinner middle region. Meanwhile, the strains near the two ends hardly change for different $A_0/A_{r(l)}$. As a result, the piezoelectric polarization P near the depletion region, shown in Figs. 7(c) and 7(d), changes most evidently with the necking of the PN junction. Further, in Fig. 7(e) for homogeneous junctions, the electric potential φ are almost unchanged for different $A_0/A_{r(l)}$ values. This is because in the middle part of the fiber, potential is totally screened by free charges although the largest strain variation is located there. While near the two ends, the strain variations are too tiny to obviously change the potential via piezoelectric effect. Unlike the case of homogeneous junctions, φ in heterogeneous junctions shown in Fig. 7(f) are much more sensitive to $A_0/A_{r(l)}$. We see that with the necking of the PN junction or the decreasing of $A_0/A_{r(l)}$, a potential barrier gradually appears at the interface. This indicates that compared with a homogeneous junction, the depletion zone in the heterogeneous junction is much easier to be manipulated by external mechanical loading, especially when it possesses a narrower middle part. Such difference is induced by the surface effective polarization charge density ρ^s on the interface that origins from the discontinuity of P [11], i.e.,

$$\rho^s = P(0^-) - P(0^+). \quad (29)$$

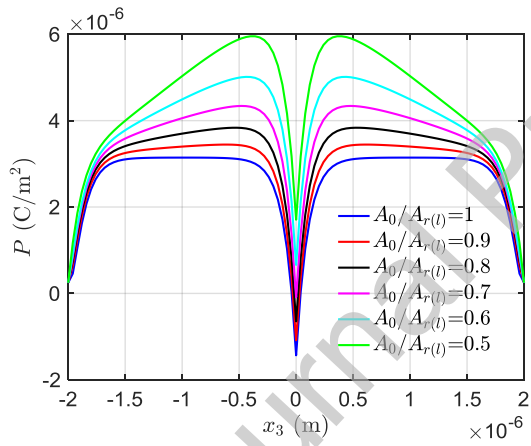
The quantitative ρ^s variation versus $A_{r(l)}/A_0$ for homogeneous and heterogeneous junctions is shown in Fig. 7(g). We see that surface effective polarization charges only exist in heterogeneous junctions (as shown in Fig. 5), and thus result in the configuration change of their depletion regions.



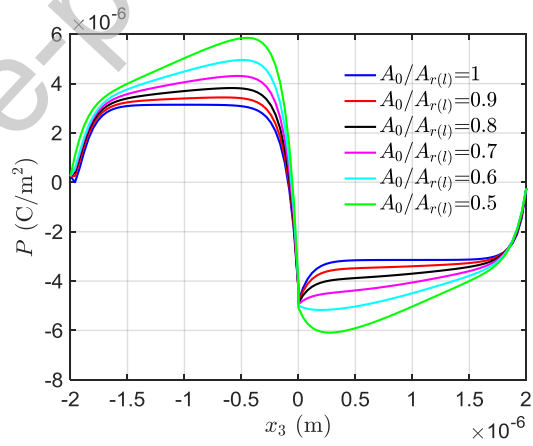
(a)



(b)



(c)



(d)

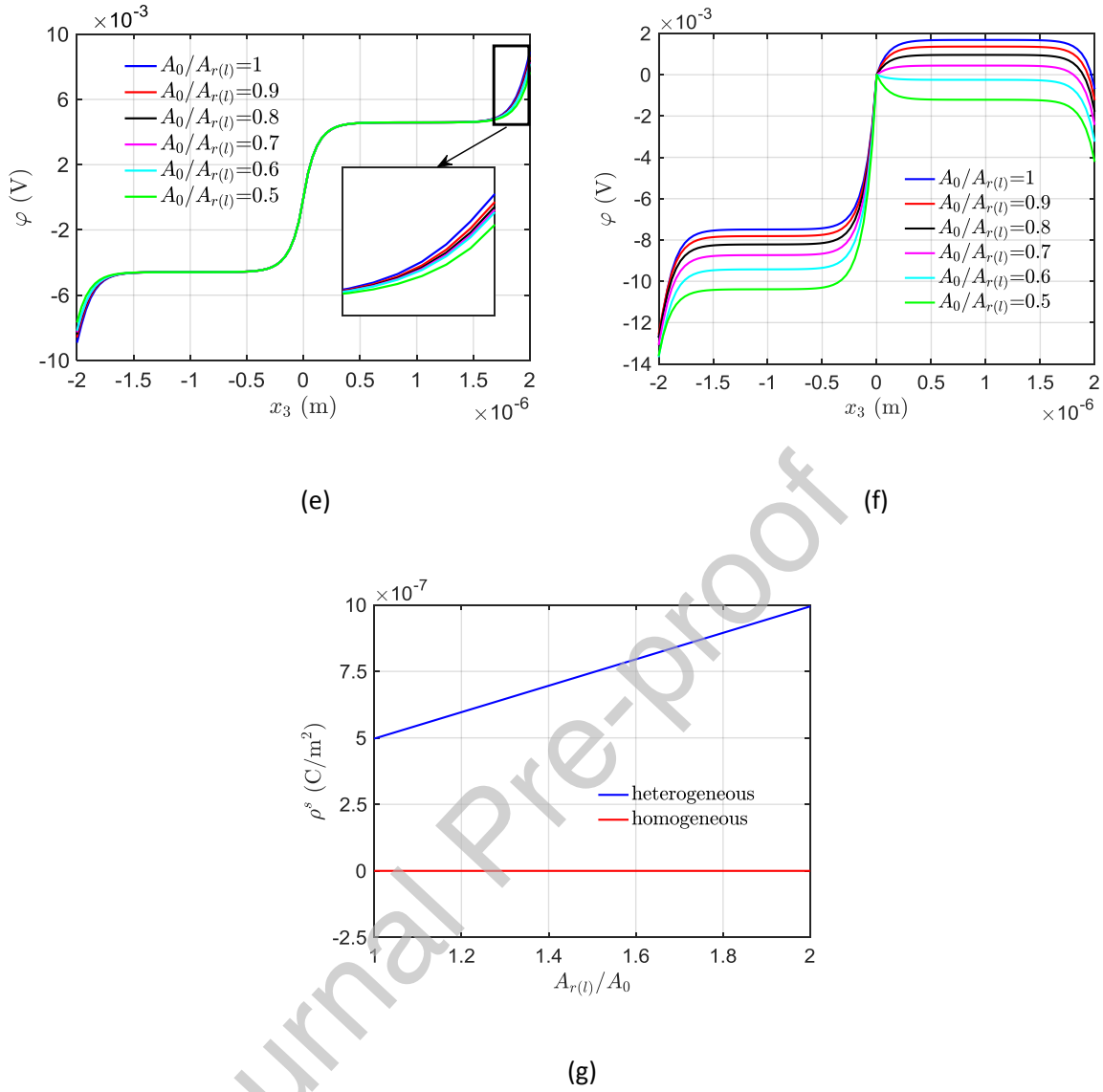


Fig. 7. Electromechanical fields in homogeneous and heterogeneous PS PN junctions for different values of cross-sectional area ratio $A_0/A_{r(l)}$. (a), (c) and (e) respectively stands for the strain S_{33} , piezoelectric polarization P , distributions of the electric potential φ in homogeneous junctions, and (b), (d), and (f) are those fields in heterogeneous junctions. (g) represents the surface effective polarization charge density ρ^s on the interface of homogeneous and heterogeneous junctions for different values of $A_{r(l)}/A_0$.

It's necessary to investigate the influence of cross-sectional area variation on the current-voltage relation (I - V curve) of a PN junction since it is closely related to the barrier configuration [37, 38]. The I - V relation is strongly nonlinear, so a COMSOL analysis is performed using the nonlinear current constitutive relations. The electrical boundary conditions applied at the two ends of the PS PN junction are

$$\varphi(-L) = V, \quad \varphi(L) = -V. \quad (30)$$

For a non-uniform heterogeneous PS PN junction with $A_0/A_{r(l)} = 0.5$, the I - V curves under different F are plotted in Fig. 8(a). It's observed that a larger applied force F leads to a smaller current, which is because it produces a higher potential barrier at the interface, making it more difficult for free carriers to smoothly flow through the junction. Furthermore, reviewing the fact shown in Fig. 7(f) that the potential barrier in a necking junction is more sensitive to F than that in a uniform one, it might be reasonable to conclude that its current-voltage relation can be tuned much more easily as well. To confirm this idea, $|\Delta I/I_0|$, the mechanical loading sensitivity of the current, for different interface areas is depicted in Fig. 8(b), in which I_0 is the current without applied force, and ΔI is the current variation deviating from $F = 0$. Results show that a smaller $A_0/A_{r(l)}$ corresponds to a larger $|\Delta I/I_0|$ for the same F , which proves that a thinner middle part of the PS PN junction leads to a higher mechanical loading sensitivity. For example, at the area ratio of 0.2, the current sensitivity is about twice that of a uniform fibre. This phenomenon is beneficial for the structural design of ultrahigh sensitive piezotronic devices based on piezotronic PN junctions.

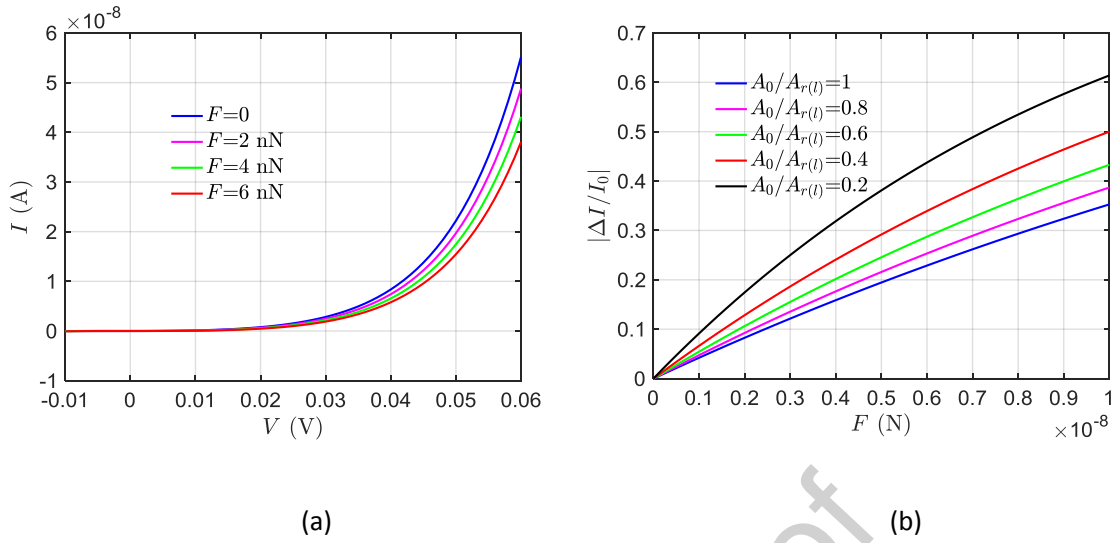


Fig. 8. (a) Current-voltage relations in a non-uniform PS PN junction for different values of F . (b) Current sensitivity curves versus F for different values of cross-sectional area ratio $A_0/A_{r(l)}$.

Recently, more and more attentions have been paid to the polycrystalline piezotronic ceramics [39-41], in which whether the interface barriers formed between adjacent nanocrystals increase, decrease or remain unmodified depends on the orientation of piezoelectric nanocrystals. Two typical simplified configurations, head-to-head and head-to-tail, are shown in Fig. 9(a), to which the power series expansion method is still applicable. Their potential distributions are shown in Figs. 9(b) and 9(c) with $n'_0 = n'_0 = 10^{21} \text{ m}^{-3}$, $p'_0 = p'_0 = 0$, and other material constants and cross-sectional area variation function are the same as those used for Fig. 7. Results demonstrate that the interface barrier in the head-to-head configuration is sensitive to the area variation, whilst that in the head-to-tail configuration isn't. The reason is similar to that for PS PN junctions, i.e., piezoelectric charges always tend to appear at the heterogeneous interface. This qualitative analysis is beneficial for the application of statistical piezotronic devices made of multiple nanoplatelets.

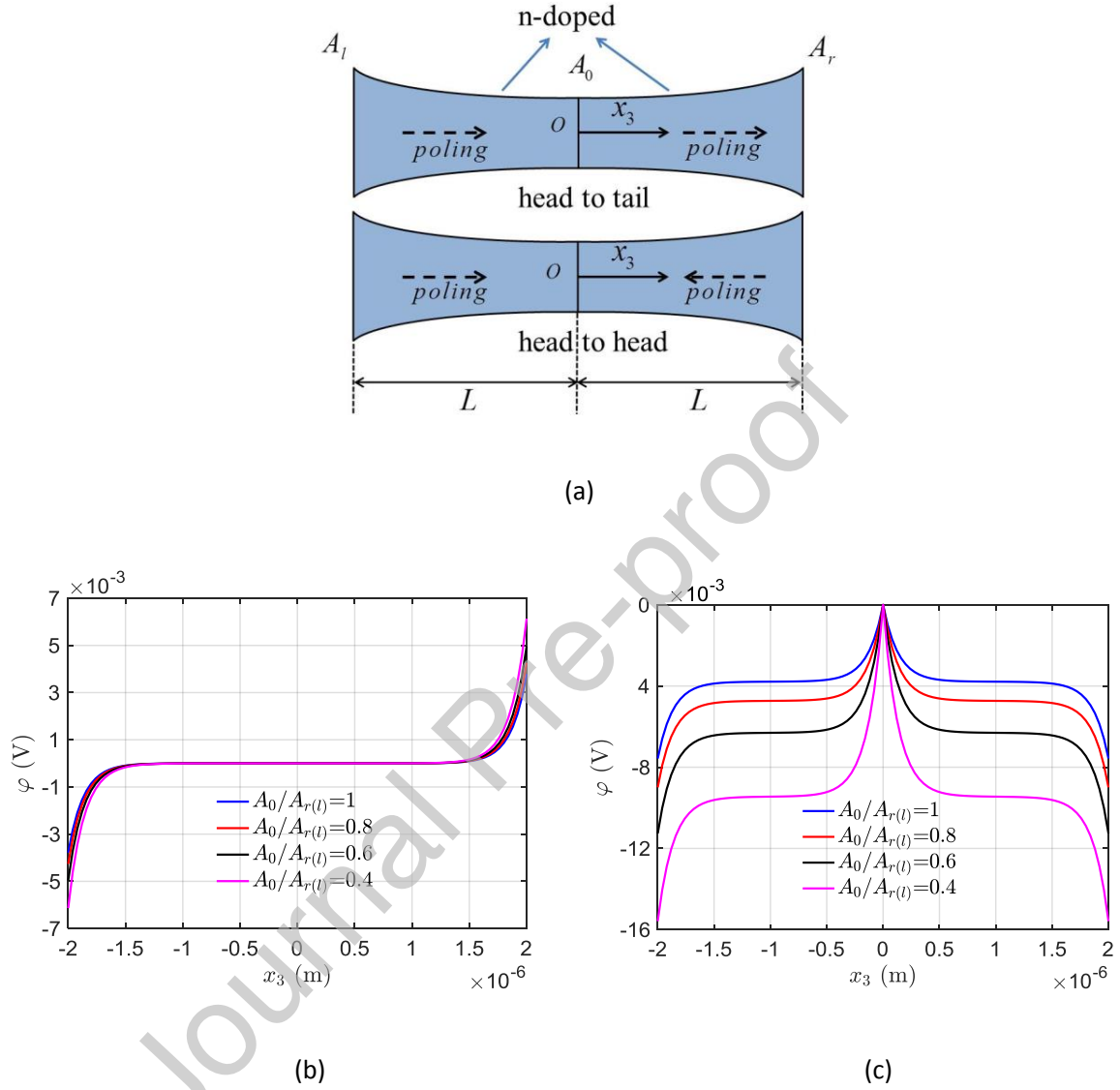


Fig. 9 (a) Schematic representation of two typical polycrystalline piezotronic configurations with head-to-head and head-to-tail orientations. Electric potential distribution φ for different values of cross-sectional area ratio $A_0/A_{r(l)}$ in (b) head-to-tail and (c) head-to-head configurations.

6. Conclusions

Based on the linearized one-dimensional coupled equations, a power series expansion method is proposed to investigate the electromechanical behaviors of non-uniform piezoelectric semiconductor (PS) fibers with variable cross sections. The carrier concentration variation and cross-sectional area variation along the axial direction are expanded into power series to obtain the semi-analytical solution of the governing equation with variable coefficients. The convergence of the method is examined respectively for uniform PS fibers and fibers with linear and quadratic forms of cross-sectional area variation. It takes fewer than 30 terms for all of the series involved to converge. The accuracy of the method is validated by comparing the semi-analytical results with those obtained from the exact analytical solution. However, three-dimensional finite element simulation shows that the proposed linearized model is only applicable to the cases of small external loading. When the mechanically induced carrier concentration variation exceeds 0.5 times the initial value, the deviation between the results of the linearized model and the numerical solution is unacceptable. This issue needs to be further investigated in future works.

The proposed power series expansion method is utilized to explore the piezotronic performance of non-uniform n-type PS fibers. The antisymmetry of the electromechanical fields in these non-uniform fibers is broken. For the fiber with linear cross-sectional area variation, when the piezo-potential near one end increases 5 times as the surface area decreases, the potential near the other end hardly changes. This is because the larger deformation of the thinner end produces more polarization charges on the surface, thus changing the field distribution nearby more drastically. Further, the power series expansion method is extended for the analysis of PS PN junctions. Results show that the potential barrier configuration and the corresponding current-voltage relation of a necking heterogeneous PS PN junction are more sensitive to mechanical loading than those of a uniform one. When the interface area

of a junction shrinks to $1/5$ of its end surface area, the sensitivity of the current to external mechanical loading increases to twice that of a uniform junction. The theoretical method herein extends the fundamental theory of piezotronics, and the qualitative phenomena and quantitative results reported enrich the structural design of high sensitivity piezotronic devices.

Acknowledgments

This work was supported by the National Natural Science Foundation of China (12061131013, 11972276, 12172171 and 12102183), the China Postdoctoral Science Foundation (2021M701704), the State Key Laboratory of Mechanics and Control of Mechanical Structures at NUAU (No. MCMS-E-0520K02), the Fundamental Research Funds for the Central Universities (NE2020002 and NS2019007), National Natural Science Foundation of China for Creative Research Groups (No. 51921003), the Start-up Fund supported by NUAU, Postgraduate Research & Practice Innovation Program of Jiangsu Province (KYCX21_0179), National Natural Science Foundation of Jiangsu Province (BK20211176), Local Science and Technology Development Fund Projects Guided by the Central Government (2021Szvup061), and a project funded by the Priority Academic Program Development of Jiangsu Higher Education Institutions (PAPD). Prof. Iren Kuznetsova and Dr. Vladimir Kolesov thank Russian Ministry of Science and Higher Education (Government task), Russian Foundation of Basic Research (grant #20-07-00139), and Russian Ministry of Science and Education (#0030-2019-0016) for financial supports.

Appendix A

In this appendix, we introduce the exact solution for the electromechanical fields in a non-uniform fiber with the cross-sectional area varying in the form of $A(x_3) = A_0(1+\alpha_2x_3/L)^2$. For this profile, Eq. (20) can be transformed into a Helmholtz equation, i.e.,

$$(\Delta n \psi)_{,33} - \kappa^2 \Delta n \psi = 0 \quad (\text{A1})$$

with

$$\psi = 1 + \alpha_2 \frac{x_3}{L}, \quad (\text{A2})$$

and its solution is

$$\Delta n \psi = \kappa C_1 \sinh(\kappa x_3) + \kappa C_2 \cosh(\kappa x_3). \quad (\text{A3})$$

Here C_1 and C_2 are undetermined coefficients that need to be derived by using of the electrical open-circuit boundary condition in Eq. (22). Then, Δn can be calculated via

$$\Delta n = \frac{\kappa C_1 \sinh(\kappa x_3) + \kappa C_2 \cosh(\kappa x_3)}{1 + \alpha_2 x_3 / L}. \quad (\text{A4})$$

Appendix B

According to relevant literatures [33, 37], the following 3D nonlinear equations for the n-type PS fiber are solved using FEM software:

$$\begin{aligned}\sigma_{ij,j} &= 0, \\ D_{i,i} &= q(N_D^+ - n),\end{aligned}\tag{A6}$$

with

$$n = n_0 \exp\left(\frac{q\varphi}{k_B T}\right).\tag{A7}$$

For the static extensional deformation considered in this paper, the current equation $J_{i,i}^0 = q\partial n/\partial t$ has been omitted here. If we still choose the state before stress applied as the reference state, the current equation is transformed into the relation of carrier concentration n and electric potential φ , i.e., Eq. (A7).

Fig. A1 shows the potential distribution φ calculated by the 3D FEM software in a cross section at $x_3 = -0.95 \mu\text{m}$ of the PS fiber, for which $A(x) = A_0(1 + \alpha_2 x_3/L)^2$, $A_r/A_r = 0.4$ and $F = 5 \text{ nN}$. It is observed that φ is non-uniform in the cross section, which deviates from the assumption of 1D linearized method. However, the variation tendency of φ in the x_1 - x_2 plane is small, and then its influence on calculation accuracy is tiny.

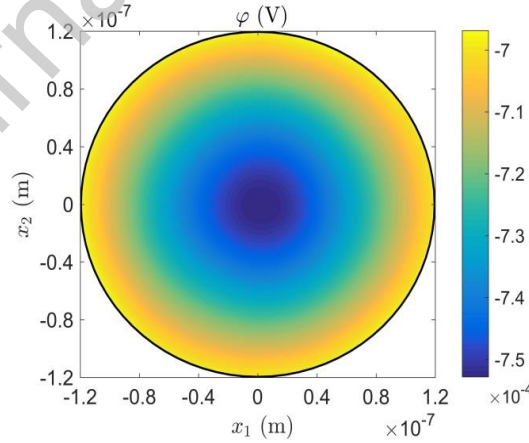


Fig. A1. The non-uniform distribution of electric potential φ in a cross section of the PS fiber.

References

- [1] Y. Qin, X.D. Wang, Z.L. Wang, Microfibre-nanowire hybrid structure for energy scavenging, *Nature*, 451 (2008) 809-813.
- [2] M.A. Johar, M.A. Hassan, A. Waseem, J.S. Ha, J.K. Lee, S.W. Ryu, Stable and high piezoelectric output of GaN nanowire-based lead-free piezoelectric nanogenerator by suppression of internal screening, *Nanomaterials*, 8 (2018) 437.
- [3] X.D. Wang, J. Zhou, J.H. Song, J. Liu, N.S. Xu, Z.L. Wang, Piezoelectric field effect transistor and nanoforce sensor based on a single ZnO nanowire, *Nano Lett.*, 6 (2006) 2768-2772.
- [4] R.S. Dahiya, G. Metta, M. Valle, A. Adami, L. Lorenzelli, Piezoelectric oxide semiconductor field effect transistor touch sensing devices, *Appl. Phys. Lett.*, 95 (2009) 034105.
- [5] J.M. Wu, K.-H. Chen, Y. Zhang, Z.L. Wang, A self-powered piezotronic strain sensor based on single ZnSnO₃ microbelts. *Rsc Adv.*, 3 (2013) 25184-25189.
- [6] J.J. Qi, H. Zhang, S.N. Lu, X. Li, M.X. Xu, Y. Zhang, High performance indium-doped ZnO gas sensor. *J. Nanomater.*, 2015 (2015) 954747.
- [7] J. Zhang, J.L. Zhou, Humidity-dependent piezopotential properties of zinc oxide nanowires: Insights from atomic-scale modelling, *Nano Energy*, 50 (2018) 298-307.
- [8] W.Z. Wu, Y.G. Wei, Z.L. Wang, Strain-gated piezotronic logic nanodevices, *Adv. Mater.*, 22 (2010) 4711-4715.

- [9] M.K. Guo, Y. Li, G.S. Qin, M.H. Zhao, Nonlinear solutions of PN junctions of piezoelectric semiconductors, *Acta Mech.*, 230 (2019) 1825-1841.
- [10] K.Y. Lee, B. Kumar, J.S. Seo, K.H. Kim, J.I. Sohn, S.N. Cha, D. Choi, Z.L. Wang, S.W. Kim, P-type polymer-hybridized high-performance piezoelectric nanogenerators, *Nano Lett.*, 12 (2012) 1959-1964.
- [11] R.R. Cheng, C.L. Zhang, W.Q. Chen, J.S. Yang, Temperature effects on PN junctions in piezoelectric semiconductor fibers with thermoelastic and pyroelectric couplings, *J. Electron. Mater.*, 49 (2020) 3140-3148.
- [12] K. Tong, C.R. Zhou, Q.N. Li, J. Wang, L. Yang, J.W. Xu, G.H. Chen, C.L. Yuan, G.H. Rao, Enhanced piezoelectric response and high-temperature sensitivity by site-selected doping of BiFeO₃-BaTiO₃ ceramics, *J. Eur. Ceram. Soc.*, 38 (2018) 1356-1366.
- [13] W.Z. Wu, L. Wang, Y.L. Li, F. Zhang, L. Lin, S.M. Niu, D. Chenet, X. Zhang, Y.F. Hao, T.F. Heinz, J. Hone, Z.L. Wang, Piezoelectricity of single-atomic-layer MoS₂ for energy conversion and piezotronics, *Nature*, 514 (2014) 470-474.
- [14] S. Lee, R. Hinchet, Y. Lee, Y. Yang, Z.H. Lin, G. Ardila, L. Montes, M. Mouis, Z.L. Wang, Ultrathin nanogenerators as self-powered/active skin sensors for tracking eye ball motion, *Adv. Funct. Mater.*, 24 (2014) 1163-1168.
- [15] P. Rajagopalan, V. Singh, I.A. Palani, S.J. Kim, Superior response in ZnO nanogenerator via interfaced heterojunction for novel smart gas purging system, *Extreme Mech. Lett.*, 26 (2019) 18-25.
- [16] Y.M. Zhang, G.W. Hu, Y. Zhang, L. Li, M. Willatzen, Z.L. Wang, High performance piezotronic devices based on non-uniform strain, *Nano Energy*, 60 (2019) 649-655.

- [17] Y.F. Hu, Y. Zhang, C. Xu, G.A. Zhu, Z.L. Wang, High-output nanogenerator by rational unipolar assembly of conical nanowires and its application for driving a small liquid crystal display, *Nano Lett.*, 10 (2010) 5025-5031.
- [18] R. Araneo, C. Falconi, Lateral bending of tapered piezo-semiconductive nanostructures for ultra-sensitive mechanical force to voltage conversion, *Nanotechnology*, 24 (2013) 265707.
- [19] R. Araneo, G. Lovat, P. Burghignoli, C. Falconi, Piezo-semiconductive quasi-1D Nanodevices with or without anti-symmetry, *Adv. Mater.*, 24 (2012) 4719-4724.
- [20] C. Ren, K.F. Wang, B.L. Wang, Adjusting the electromechanical coupling behaviors of piezoelectric semiconductor nanowires via strain gradient and flexoelectric effects, *J. Appl. Phys.*, 128 (2020) 215701.
- [21] H.Y. Huang, Z.H. Qian, J.S. Yang, Mechanical manipulation of electrical behaviors of piezoelectric semiconductor nanofibers by time-dependent stresses, *Acta Mech. Solida Sin.*, 33 (2020) 579-585.
- [22] P. Li, F. Jin, J.S. Yang, Effects of semiconduction on electromechanical energy conversion in piezoelectrics, *Smart Mater. Struct.*, 24 (2015) 025021.
- [23] F.Y. Jiao, P.J. Wei, Y.H. Zhou, X.L. Zhou, Wave propagation through a piezoelectric semiconductor slab sandwiched by two piezoelectric half-spaces, *Eur. J. Mech. A-Solids*, 75 (2019) 70-81.
- [24] N. Li, Z.H. Qian, J.S. Yang, Effects of edge and interior stresses on electrical behaviors of piezoelectric semiconductor films, *Ferroelectrics*, 571 (2021) 96-108.
- [25] M.H. Zhao, Q.Y. Zhang, C.Y. Fan, An efficient iteration approach for nonlinear boundary value problems in 2D piezoelectric semiconductors, *Appl. Math. Model.*, 74 (2019) 170-183.

- [26] X. Guo, P.J. Wei, Dispersion relations of in-plane elastic waves in nano-scale one dimensional piezoelectric semiconductor/piezoelectric dielectric phononic crystal with the consideration of interface effect, *Appl. Math. Model.*, 96 (2021) 189-214.
- [27] B.R.F. Pierret, *Semiconductor fundamentals*, Addison-Wesley, 1989.
- [28] H.F. Tiersten, *Linear Piezoelectric Plate Vibrations*, Plenum Press, 1969.
- [29] C.L. Zhang, X.Y. Wang, W.Q. Chen, J.S. Yang, Carrier distribution and electromechanical fields in a free piezoelectric semiconductor rod, *J. Zhejiang Univ.-SCI A*, 17 (2016) 37-44.
- [30] C.L. Zhang, X.Y. Wang, W.Q. Chen, J.S. Yang, An analysis of the extension of a ZnO piezoelectric semiconductor nanofiber under an axial force, *Smart Mater. Struct.*, 26 (2017) 025030.
- [31] R.R. Cheng, C.L. Zhang, W.Q. Chen, J.S. Yang, Piezotronic effects in the extension of a composite fiber of piezoelectric dielectrics and nonpiezoelectric semiconductors, *J. Appl. Phys.*, 124 (2018) 064506.
- [32] Y. Guo, C. Zhang, W. Chen, J. Yang, Interaction between torsional deformation and mobile charges in a composite rod of piezoelectric dielectrics and nonpiezoelectric semiconductors. *Mech. Adv. Mater. Struct.* (2020) in press.
- [33] W.L. Yang, Y.T. Hu, E.N. Pan, Tuning electronic energy band in a piezoelectric semiconductor rod via mechanical loading, *Nano Energy*, 66 (2019) 104147.
- [34] G.L. Wang, J.X. Liu, X.L. Liu, W.J. Feng, J.S. Yang, Extensional vibration characteristics and screening of polarization charges in a ZnO piezoelectric semiconductor nanofiber, *J. Appl. Phys.*, 124 (2018) 094502.
- [35] G.Y. Yang, L. Yang, J.K. Du, J. Wang, J.S. Yang, PN junctions with coupling to bending deformation in composite piezoelectric semiconductor fibers, *Int. J. Mech. Sci.*, 173 (2020) 105421.

- [36] Y.X. Luo, C.L. Zhang, W.Q. Chen, J.S. Yang, An analysis of PN junctions in piezoelectric semiconductors, *J. Appl. Phys.*, 122 (2017) 204502.
- [37] W.L. Yang, J.X. Liu, Y.T. Hu, Mechanical tuning methodology on the barrier configuration near a piezoelectric PN interface and the regulation mechanism on I-V characteristics of the junction, *Nano Energy*, 81 (2021) 105581.
- [38] Y. Liu, Y. Zhang, Q. Yang, S.M. Niu, Z.L. Wang, Fundamental theories of piezotronics and piezophotonics, 14 (2015) 257-275.
- [39] P. Keil, M. Trapp, N. Novak, T. Fromling, H.J. Kleebe, J. Rodel, Piezotronic tuning of potential barriers in ZnO bicrystals, *Adv. Mater.*, 30 (2018) 1705573.
- [40] S.H. Liu, M. Han, X.L. Feng, Q.H. Yu, L. Gu, L.F. Wang, Y. Qin, Z.L. Wang, Statistical piezotronic effect in nanocrystal bulk by anisotropic geometry control, *Adv. Funct. Mater.*, 31 (2021) 2010339.
- [41] K.A. Taylor, E. Gjonaj, Z. Zhou, B. Xu, Mesoscopic modeling of the mechanically tunable electrical conductivity of ZnO varistors, *J. Appl. Phys.*, 127 (2020) 155104.